CORA Cork Open Research Archive
Cartlann Taighde Oscailte Chorcaí

| Title | Propagation of nanopores during anodic etching of n-InP in KOH |
| --- | --- |
| Authors | Lynch, Robert P.;Quill, Nathan;O'Dwyer, Colm;Nakahara, Shohei;Buckley, D. Noel |
| Publication date | 2013-08-28 |
| Original Citation | Lynch, R. P., Quill, N., O'Dwyer, C., Nakahara, S. and Buckley, D. N. (2013) 'Propagation of nanopores during anodic etching of n-InP in KOH', Physical Chemistry Chemical Physics, 15(36), pp. 15135-15145. |
| Type of publication | Article (peer-reviewed) |
| Link to publisher's version | http://pubs.rsc.org/en/content/articlelanding/2013/cp/c3cp52253a - 10.1039/C3CP52253A |
| Rights | © the Owner Societies 2013. Royal Society of Chemistry |
| Download date | 2024-04-18 02:38:52 |
| Item downloaded from | http://dx.doi.org/10.1039/C3CP52253A |

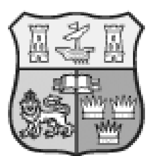

UCC
University College Cork, Ireland
Coláiste na hOllscoile Corcaigh

View Article Online
View Journal

PCCP

# Accepted Manuscript

This article can be cited before page numbers have been issued, to do this please use: R. P. Lynch, N. Quill, C. ODwyer, S. Nakahara and D. N. Buckley, *Phys. Chem. Chem. Phys.*, 2013, DOI: 10.1039/C3CP52253A.

This is an *Accepted Manuscript*, which has been through the RSC Publishing peer review process and has been accepted for publication.

*Accepted Manuscripts* are published online shortly after acceptance, which is prior to technical editing, formatting and proof reading. This free service from RSC Publishing allows authors to make their results available to the community, in citable form, before publication of the edited article. This *Accepted Manuscript* will be replaced by the edited and formatted *Advance Article* as soon as this is available.

To cite this manuscript please use its permanent Digital Object Identifier (DOI®), which is identical for all formats of publication.

More information about *Accepted Manuscripts* can be found in the **Information for Authors**.

Please note that technical editing may introduce minor changes to the text and/or graphics contained in the manuscript submitted by the author(s) which may alter content, and that the standard **Terms & Conditions** and the **ethical guidelines** that apply to the journal are still applicable. In no event shall the RSC be held responsible for any errors or omissions in these *Accepted Manuscript* manuscripts or any consequences arising from the use of any information contained in them.

RSC Publishing

www.rsc.org/pccp
Registered Charity Number 207890

Journal Name

Dynamic Article Links ►
View Article Online
DOI: 10.1039/C3CP52253A

Cite this: DOI: 10.1039/c0xx00000x

www.rsc.org/xxxxxx

ARTICLE TYPE

Published on 31 July 2013. Downloaded by University College Cork on 07/08/2013 15:00:57.

Physical Chemistry Chemical Physics Accepted Manuscript

# Propagation of Nanopores during Anodic Etching of n-InP in KOH

**Robert P. Lynch,*[a] Nathan Quill,[a] Colm O'Dwyer,[a,b] Shohei Nakahara[a] and D. Noel Buckley[a]**

***Received (in XXX, XXX) Xth XXXXXXXXX 20XX, Accepted Xth XXXXXXXXX 20XX***
**DOI: 10.1039/b000000x**

We propose a three-step model of electrochemical nanopore formation in n-InP in KOH that explains how crystallographically oriented etching can occur even though the rate-determining process (hole generation) occurs only at pore tips. The model shows that competition in kinetics between hole diffusion and electrochemical reaction determines the average diffusion distance of holes along the semiconductor surface and this, in turn, determines whether etching is crystallographic. If the kinetics of reaction are slow relative to diffusion, etching can occur at preferred crystallographic sites within a zone in the vicinity of the pore tip, leading to pore propagation in preferential directions. Symmetrical etching of three {111}A faces forming the pore tip causes it to propagate in the (remaining) <111>A direction. As a pore etches, propagating atomic ledges can meet to form sites that can become new pore tips and this enables branching of pores along any of the <111>A directions. The model explains the observed uniform width of pores and its variation with temperature, carrier concentration and electrolyte concentration. It also explains pore wall thickness, and deviations of pore propagation from the <111>A directions. We believe that the model is generally applicable to electrochemical pore formation in III-V semiconductors.

## Introduction

Nanotechnology is an area of growing industrial importance.[1] In particular there is considerable interest in the fabrication and characterisation of nano-scale structures for various applications. Although considerable progress has been made in developing technology for such applications, the underlying fundamentals are not always well understood and many important scientific questions need to be investigated if technological progress is to be maintained. Fundamental studies of key processes such as nanopore formation therefore provide important pathways to understanding and controlling nanofabrication techniques.

Nanopore formation due to electrochemical etching occurs in a range of semiconductors from Si to InP [2-8] and it is quite common for such pores to propagate along preferential directions. These directions and the pore morphology have been shown to be affected by a range of parameters including temperature,[9] composition[10,11] and concentration[12] of electrolyte, and type,[13] orientation[14] and doping density[15] of the substrate. Many different pore morphologies have been observed and several models have been proposed[16-27] to explain them; however most models address only specific combinations of semiconductor and electrolyte.

It is generally accepted that the propagation of nanopores in highly doped n-type semiconductors is controlled by hole generation under the influence of a high electric field due to the small radius of curvature at the pore tip. Zhang[26,27] modelled the relationship between pore-tip shape and electric field in silicon and showed that the electric field at the surface is sufficiently enhanced by the pore-tip's curvature to enable substantial tunnelling of carriers. This results in significant etching occurring only at pore-tips, allowing continued propagation of these tips into the substrate.

Etching of III-V semiconductors is often observed to be anisotropic. For example both chemical[28-31] and electrochemical[32,33] etching of III-V semiconductors show preferential etching of {111}B planes (*i.e.* group-V-terminated planes). The slowest-etching plane is usually {111}A and so these facets are revealed during etching of InP,[34,35] GaAs[33,36,37] and GaP.[30] Due to the differing etch rates of crystal planes, the formation of tetrahedral etch pits (seen as dove-tailed and v-groove voids, respectively, in (011) and $(01\bar{1})$ cross sections) is observed on the (100) surface of III-V semiconductors.[31,35,36]

We have previously investigated[38-43] the early stages of pore formation in InP in aqueous KOH electrolytes. Pores originate from pits in the surface and propagate along <111>A directions to form porous domains beneath a thin near-surface layer penetrated only by the surface pits.[40] Eventually these domains merge to create a continuous porous layer.[43] Although pore propagation in InP in KOH is usually crystallographically oriented (CO), it can be current-line-oriented (CLO) under certain conditions.[41] Indeed, variation of potential, electrolyte concentration and temperature causes a gradual change in the porous layer structure and a transition from pore formation to planar etching is observed as the KOH concentration is decreased to below 2 mol dm$^{-3}$.[9,44]

In this paper we examine why pore propagation is crystallographically oriented even though the etching is controlled by hole generation at pore tips. We propose a three-step model based on competitive kinetics between electrochemical reaction and hole diffusion. The model is

View Article Online
DOI: 10.1039/C3CP52253A

Published on 31 July 2013. Downloaded by University College Cork on 07/08/2013 15:00:57.

supported by a variety of scanning and transmission electron microscopy (SEM and TEM) observations of InP electrodes anodised under various conditions.

## Experimental

Wafers were monocrystalline, sulfur-doped, n-type indium phosphide (n-InP) grown by the liquid-encapsulated Czochralski (LEC) method and supplied by Sumitomo Electric. They were polished on one side and had a surface orientation of (100) and a carrier concentration in the range 3–7 × $10^{18}$ $cm^{-3}$. To fabricate working electrodes, wafers were cleaved into coupons along the natural {011} cleavage planes. Ohmic contact was made by alloying indium to the back of a coupon; the back and the cleaved edges were then isolated from the electrolyte by means of a suitable varnish. The electrode area was typically 0.2 $cm^2$. Prior to immersion in the electrolyte, the working electrode was immersed in a piranha etchant (3:1:1 $H_2SO_4$:$H_2O_2$:$H_2O$) for 4 minutes and then rinsed with deionized water.

Anodisation was carried out in aqueous KOH electrolytes in the absence of light using a linear potential sweep (LSV) at 2.5 mV $s^{-1}$. A conventional three-electrode cell configuration was used, employing a platinum counter electrode and a saturated calomel electrode (SCE) to which all potentials are referenced. A CH Instruments Model 650A Electrochemical Workstation interfaced to a Personal Computer (PC) was employed for cell parameter control and for data acquisition.

Cleaved (01$\bar{1}$) and (0$\bar{1}\bar{1}$) cross sections of electrodes were examined using a Hitachi S-4800 field-emission scanning electron microscope (FE SEM) operating at 5 kV, unless otherwise stated. Electron-transparent sections for plan-view and cross-sectional transmission electron microscopy (TEM) examination were prepared using standard focused ion beam (FIB) milling procedures[45] in an FEI 200 FIB workstation. The TEM characterization was performed using a JEOL 2011 transmission electron microscope operating at 200 kV.

## Results and Discussion

### Characteristics of Anodic Pore Formation in InP in KOH

Figure 1 shows a typical linear sweep voltammogram (LSV) for the anodisation of n-InP in 5 mol $dm^{-3}$ KOH. Negligible current flow is observed at low potentials. This behaviour is typical of n-type semiconductors anodised in the dark as the surface is depleted of charge carriers and electrochemical reaction is therefore inhibited. When a characteristic potential (~0.4 V in the present case) is reached, the current increases rapidly. This onset of current has been shown [38,40] to correspond to the formation of etch pits in the electrode surface.

The SEM images in Fig. 2 show the general features of nanopore growth. As is typically observed, two pores (which we call primary pores) originate from each surface pit and propagate along <111>A directions.[38] Two such primary pores can be seen in the SEM image in Fig. 2a, which shows a typical {011} cross section through an InP wafer anodised up to point B in Fig. 1. As these pores continue to propagate into the InP substrate, many more pores branch off from them, forming a porous domain. These porous domains eventually merge together to form a continuous porous layer beneath the electrode surface (as in Fig. 2a). Fig. 2b shows a typical {011} cross section through an InP wafer anodised up to A in Fig. 1, a point before domains had merged into a continuous layer. Thus, individual porous domains

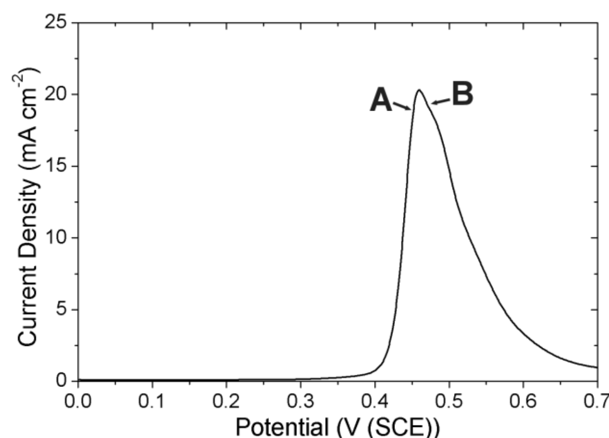


**Fig. 1** LSV of an n-InP electrode in 5 mol $dm^{-3}$ KOH (n ≈ 3.4 × $10^{18}$ $cm^{-3}$). The potential was scanned from 0 to 0.7 V (SCE) at a scan rate of 2.5 mV $s^{-1}$ at room temperature.

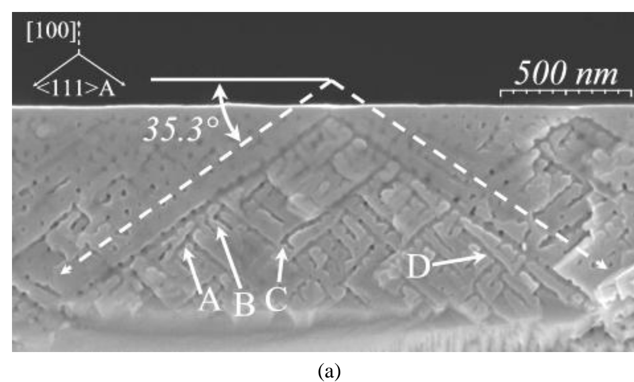


(a)

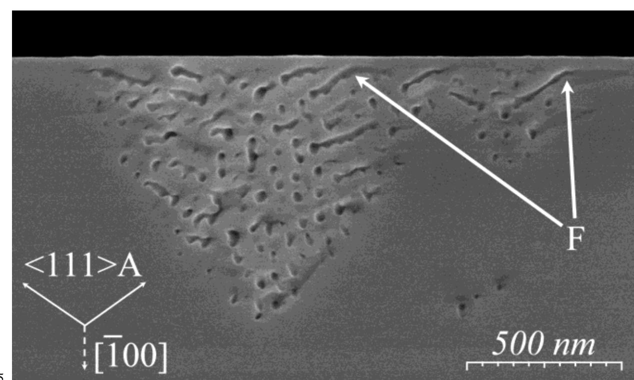


(b)

**Fig. 2** Cross-sectional {011} SEM images of InP following anodisation by LPS at 2.5 mV $s^{-1}$ from 0 V (SCE) to (a) 0.46 V (point B in Fig. 1) and (b) 0.44 V (point A in Fig. 1). The <111>A directions are indicated on the images. Image (a) shows a (011) cross section, which we refer to as an α plane, with pores propagating along <111>A directions. Pores that deviate from these directions are indicated at A and D and pores that have avoided crossing other pores are indicated at B and C. Image (b) shows a (01$\bar{1}$) plane (*i.e.* orthogonal to (a)), which we refer to as a β plane. Pores propagating in α planes (such as the pores in (a)) appear as round cross-sections. Pores in the plane of the image propagate upwards at ~35° to the horizontal plane along the <111>A directions. Pores that have deviated from the <111>A directions as they approached the electrode surface are indicated at F.

Physical Chemistry Chemical Physics Accepted Manuscript

 This journal is © The Royal Society of Chemistry [year]

View Article Online
DOI: 10.1039/C3CP52253A

Published on 31 July 2013. Downloaded by University College Cork on 07/08/2013 15:00:57.

are visible. The characteristic triangular cross-sections of these domains [39] is apparent: the cleavage plane (β plane)[38] is orthogonal to that in Fig. 2a (*α* plane). Many of the pores in Fig. 2b are passing through the image plane (they are growing in the perpendicular *α* plane) and so appear as circular features ('holes in the plane'). However, some pores are also observed in the β plane of the image and these have grown in a <111>A direction towards the surface. Thus, pore branching occurs both downward in the *α* plane and upward in the β plane (*i.e.* along all four <111>A directions). We have previously shown in detail that the pore patterns predicted for these growth directions are in good agreement with SEM and TEM observations.[38]

More detailed examination of Fig. 2a, particularly the relatively long primary pores, reveals that the width of pores is constant along their length, *i.e.* no tapering is evident. This observation strongly suggests that all etching occurs in a very small volume near the pore tip. We infer that, as this region advances, there is no subsequent etching of pore walls since any such etching would be expected to lead to tapered pores, wider closer to the surface because of longer etching times. This also means that there must be no chemical etching of pore walls unlike other systems [46,47] where the observation of tapered pores suggests that some chemical etching takes place in parallel with the electrochemical etching near pore tips.

Thus, the InP/KOH system appears to be an ideal system for the study of purely electrochemical nanopore formation where all of the etching is confined to the vicinity of each pore tip. We now propose a model to explain the propagation of pores along the <111>A directions.

## Towards a Model of Pore Formation in InP

In order to electrochemically etch a semiconductor, free charge carriers (electrons or holes) must be present at the semiconductor surface. Furthermore, charge carriers must be sufficiently energetic to induce an etching reaction.[48] It has been shown that for most semiconductors in contact with aqueous electrolytes, valence band holes meet this energy criterion while conduction band electrons do not.[49,50] Thus p-type semiconductors can be readily etched electrochemically.[51] However in order to electrochemically etch n-type semiconductors a source of holes is required. Such holes may be supplied by illumination or by electric-field assisted tunnelling; or they may be injected from external chemical species, either in solution or adsorbed on the semiconductor surface.[52]

Pores form and propagate if etching is much faster near their tips than elsewhere on the surface. A number of different mechanisms can lead to preferential etching at pore tips. Chemical mechanisms rely on differing etch rates between passivated pore walls and freshly revealed (unpassivated) pore tips.[17,53,54] Physical mechanisms generally rely on enhanced surface curvature at the pore tip leading to a higher local electric field which, in the case of semiconductors, allows tunnelling of charge carriers across the depletion layer.[17,21,26] Such field-assisted tunnelling has been proposed as the mechanism of hole generation during pore formation in highly doped n-type semiconductors in the dark.[2] Thus the electrochemical formation of porous InP occurs as a result of hole generation at pore tips under the influence of the curvature-enhanced electric-field at those specific sites.[55,56] In other words, the rate-determining step must be the supply of holes to the semiconductor surface which occurs at a significant rate only at the pore tips and leads to etching there in preference to other sites.

As noted above, pores are often observed to propagate along the <111>A directions and such crystallographically oriented (CO) pores have been reported both for InP [38,46] and for other III-V semiconductors.[3,19] Likewise, as discussed in the introduction, etching of III-V semiconductors is often observed to be anisotropic, typically revealing slow-etching {111}A facets. Preferential etching of crystal facets is expected when the chemical or electrochemical reaction at the surface is the rate-determining step.[33] On the other hand, preferential etching of facets is not expected where the rate-determining step is independent of surface reaction such as, for example, mass transport in the electrolyte.[29,58]

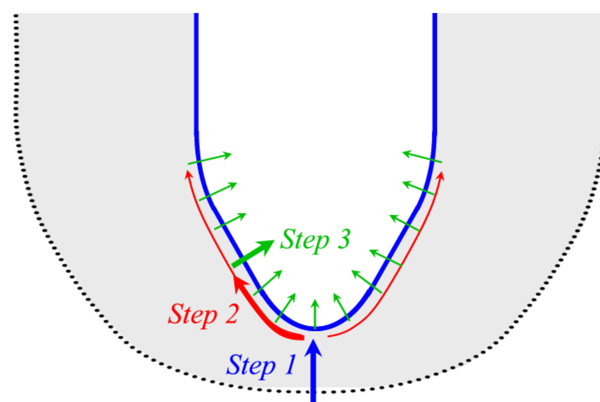


**Fig. 3** Schematic representation (not to scale) of a pore near its tip showing the three steps of the model of competitive kinetics: (Step 1) hole generation at pore tips by tunnelling of carriers (holes) across the depletion layer (shaded region); (Step 2) hole diffusion at the surface; and (Step 3) electrochemical oxidation of the semiconductor to form etch products.

Thus the formation of CO pores suggests that etching is controlled by the relative rates of the surface reactions at different facets: any satisfactory model of electrochemical pore formation must explain how this can occur even though the rate-determining process (hole generation) occurs only at pore tips. To reconcile these requirements, we propose a three-step model. The three steps (which are illustrated schematically in Fig. 3) are: (1) hole generation at pore tips, (2) hole diffusion and (3) electrochemical oxidation of the semiconductor to form etch products.

### A Three-Step Model and Competitive Kinetics

Step 1 is the generation of holes at pore tips. As discussed above, this is rate-determining and occurs under the influence of a high electric field due to the small radius of curvature at the pore tip.[26,27] If each hole formed were to be immediately consumed in an electrochemical reaction, then the resulting etching would be confined to a very small area at the pore tip. This would tend to further sharpen the pore tip and therefore further hole generation and etching reaction would also be confined to that specific site. The question therefore arises as to how pore propagation can occur preferentially along crystallographic directions if the rate-determining step occurs at a non-crystallographically defined site *i.e.* the pore tip.

Physical Chemistry Chemical Physics Accepted Manuscript

View Article Online
DOI: 10.1039/C3CP52253A

Published on 31 July 2013. Downloaded by University College Cork on 07/08/2013 15:00:57.

The answer must lie in Step 2: hole diffusion. If holes diffused only a negligible distance, etching would be confined to the site on the surface where they were created. However, when holes may diffuse parallel to the surface of the semiconductor, the electrochemical etching reaction may occur some distance from the pore tip where the holes are created and, as discussed below, this may lead to CO pore formation. Such diffusion of holes from their points of generation to the points where etching ultimately occurs has been reported [33,59] for photoanodic etching of n-type III-V semiconductors where etching was observed to extend beyond the illuminated region.

Step 3 is the actual electrochemical reaction itself. While the detailed chemistry and mechanism of this have not yet been elucidated, it involves oxidation of InP to indium and phosphorus species dissolved in the electrolyte within a pore. The kinetics of Step 3 do not directly determine the overall etch rate of a pore: this is determined by the rate of generation of holes at the pore tip (Step 1). However, competition in kinetics[33,59,60] between hole diffusion (Step 2) and electrochemical reaction (Step 3) is the principal factor determining the average diffusion distance of holes.

If the kinetics of Step 3 (oxidation reaction) are slow relative to Step 2 (diffusion), then holes can diffuse a significant distance before being annihilated in the oxidation reaction. Then etching can occur at preferred crystallographic sites, such as phosphorus dangling bonds in InP, within a zone in the vicinity of the pore tip and will lead to pore propagation in preferential directions. On the other hand, if the kinetics of Step 3 were fast relative to Step 2, the diffusion distance of holes would be short as they would be annihilated in the oxidation reaction close to where they were created. In that case, etching would occur close to the site of hole generation rather than at preferred crystallographic sites and so there would then be no preferred crystal direction for pore propagation.

## Mechanism of Crystallographic Etching of Pores

When the kinetics of Step 3 are sufficiently slow that holes can diffuse to crystallographically preferred reaction sites, etching will eventually reveal the slowest etching crystal facets – the {111}A facets – to form a pyramidal shape with its apex as the pore tip, as shown in Fig. 4. These {111}A planes are terminated by indium atoms, each bonded to three underlying phosphorous atoms. Removal of an indium atom therefore exposes three phosphorous atoms, each with a dangling bond as shown in Fig. 5a. Such a phosphorus atom is easily etched, breaking a bond to each of three indium atoms, two of which are surface atoms. Each of these now has two dangling bonds (each already had one) and consequently is easily etched, revealing two new phosphorous atoms, each with a dangling bond.

Phosphorous atoms with single dangling bonds can be considered to be part of a {111}B surface oriented normal to the bonds.[61] Thus, the removal of a single indium atom from a {111}A surface creates three monatomic ledges with {111}B faces, each at an angle of 109.47° to the surface as shown in Fig. 5b. Etching of the phosphorous atoms on these ledges, and the associated indium atoms, causes the ledges to advance, consequently increasing the size of the three sided region where the next underlying {111}A plane is exposed (Fig. 6).

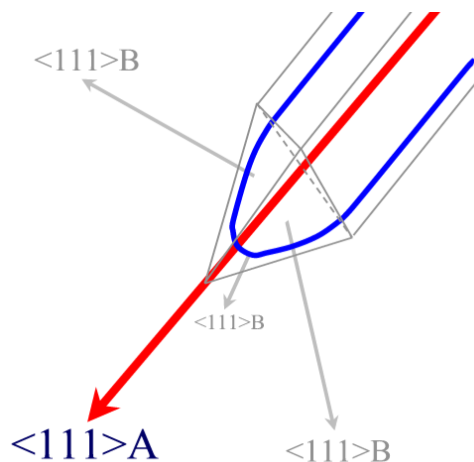


**Fig. 4** Schematic representation (not to scale) of a pore formed by the etching mechanism described in Fig. 3. The idealized shape with three {111}A facets is represented by grey lines (▬). The actual pore (represented by blue lines (▬) will have finite radius of curvature at the tip and will generally have rounded pore walls.

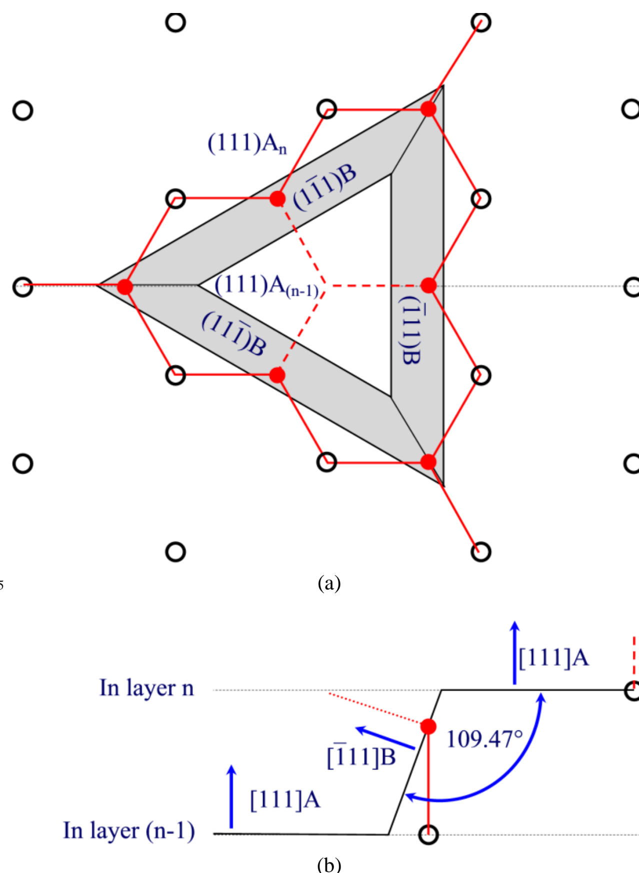


**Fig. 5** (a) An In vacancy (⁝) on a {111}A surface creating three dangling P bonds (▮▮▮▮). These P atoms (●) correspond to a {111}B monatomic ledge on three sides of the vacancy (projections of which on the {111}A plane are shown). Indium atoms are shown as open circles (○). (b) Cross-sectional view orthogonal to the surface {111}A plane and through the In vacancy and one of the P atoms in a plane containing its dangling bond. The surface {111}A plane (n) and the next underlying {111}A plane (n-1) are shown. The {111}B ledge is represented at an angle of 109.47° to the surface plane and contains the P atom with its dangling bond towards the In vacancy and normal to the surface of the ledge. Note that the P atom is bonded to an In atom in the n-1 plane; as can be seen in (a) it is also bonded to two In atoms in the n plane.

Physical Chemistry Chemical Physics Accepted Manuscript


This journal is © The Royal Society of Chemistry [year]

View Article Online
DOI: 10.1039/C3CP52253A

Published on 31 July 2013. Downloaded by University College Cork on 07/08/2013 15:00:57.

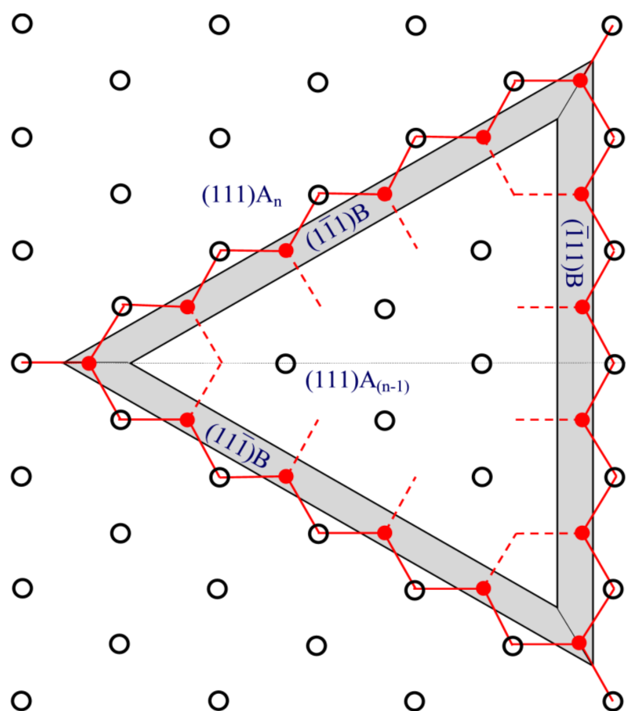


**Fig. 6** Expanded three-sided region as etching progresses further away from the original In vacancy shown in Fig. 5. This occurs as follows: as the P atoms on the ledges in Fig. 5a are etched, In atoms with two dangling bonds are exposed which in turn etch. The corner P atoms (which originally had no dangling bonds) are then exposed and etch. Thus each ledge advances to the next row of P atoms.

New vacancy sites are not formed easily but, once formed, they expand as in Fig. 6 by rapid two-dimensional etching along the surface to expose the next {111}A plane. Eventually, an indium vacancy forms in the newly exposed {111}A face and the etching process continues to expose the next underlying {111}A plane (as before, see Fig. 5). Thus, in the vicinity of the pore tip, the {111}A faces are etched, one monolayer at a time, so that the region in the vicinity of the tip maintains its pyramidal shape, and so the tip remains sharp as it propagates. Symmetrical etching of the three {111}A faces forming the tip causes it to propagate in the (fourth) <111>A direction.

The crystallographic etching that maintains {111}A facets in the vicinity of the tip is controlled by the supply of holes diffusing from the tip. The hole concentration at the surface of the facets decreases with distance from the tip, both because of divergence of the diffusing flux and because of consumption of holes in the oxidation reaction. Thus, at some distance from the tip the rate of etching becomes negligibly small. At intermediate distances, a transition region from etching to non-etching must therefore exist where propagation of ledges on individual planes ceases and where the surface curves away from the {111}A facets towards the central axis of the pore (see inset of Fig. 7).

Thus, as a pore etches multiple ledges are propagating outwards from multiple initiation points (indium vacancies) on each of the facets. Where these propagating ledges meet they can form three-sided corners at which the local electric field is sufficiently high that hole generation can occur. These sites can become new pore tips when they develop in locations sufficiently far from the depletion regions around adjacent pores. In this way, branching of pores can occur along any of the <111>A directions.

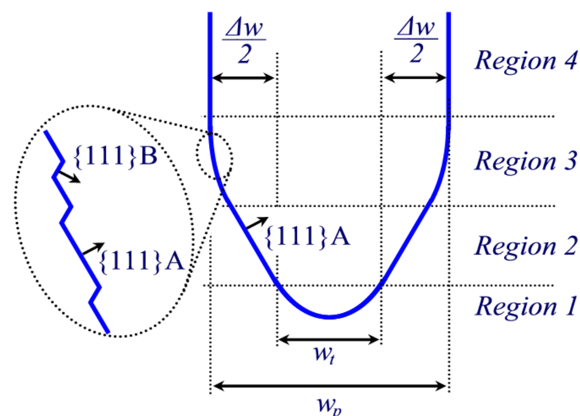


**Fig. 7** Schematic representation (not to scale) of the different regions of the pore. Region 1 is the high curvature region where hole generation occurs. Region 2 consists of three {111}A facets and Region 3 is intermediate between Region 2 and the pore walls (Region 4). In Region 3, the surface of the pore is stepped as shown in the inset and curves away from the {111}A facets as etching slows. No etching occurs in Region 4.

In summary, the three-step model can explain how the concept of rate control by localized hole generation at pore tips can be reconciled with CO etching. If Step 3 (oxidation reaction) is sufficiently fast that Step 1 (hole generation) is rate-determining but sufficiently slow in comparison with Step 2 (diffusion) that holes can diffuse a significant distance, then preferential etching of {111}B faces can occur. This leads to the formation of a faceted pore tip region which, through etching of {111}A planes one monolayer at a time, will lead to the propagation and branching of pores along <111>A directions.

## Factors Affecting Pore Width

In our model, the width $w_p$ of a pore is determined by the width $w_t$ of the tip (Region 1 in Fig. 7) and an additional width $\Delta w$ due to diffusion of holes before reaction, *i.e.* $w_p = w_t + \Delta w$ (see Fig. 7). The tip width $w_t$ is determined primarily by the radius of curvature at which the electric field reaches the threshold for hole generation and this depends primarily on the thickness of the depletion layer.[26,27] Thus $w_t$ is not expected to vary significantly for a given carrier concentration. Since $\Delta w$ depends on the diffusion distance of holes, it is predicted to increase with faster diffusion but to decrease with faster electrochemical reaction. An increase in temperature should increase the rate of electrochemical reaction more than the rate of diffusion since the activation energy for reaction is expected to be significantly larger than the activation energy for diffusion. Consequently, with increasing temperature the diffusion distance of holes, and therefore the pore width, should decrease.

**Table 1** Variation of average pore width (for n~90 measurements per sample) with temperature for n-InP (n ≈ 5.3 × $10^{18}$ $cm^{-3}$) anodised by LPS at 2.5 mV $s^{-1}$ in 9 mol $dm^{-3}$ KOH.

| Temperature / °C | 10 | 20 | 25 | 30 | 40 | 50 |
|---|---|---|---|---|---|---|
| Pore Width / nm | 38 | 33 | 31 | 28 | 27 | 26 |
| Standard Deviation / nm | 3.4 | 2.3 | 3.9 | 2.1 | 2.1 | 2.1 |

The experimental evidence supports this prediction.[9,39] Figure 8 compares SEM images of pores formed during anodisation of InP in 9 mol $dm^{-3}$ KOH at 10°C and 40°C. It is seen that the pores are significantly narrower at the higher temperature.



Physical Chemistry Chemical Physics Accepted Manuscript

View Article Online
DOI: 10.1039/C3CP52253A

Published on 31 July 2013. Downloaded by University College Cork on 07/08/2013 15:00:57.

Measurements of pore width were obtained from micrographs such as those in Fig. 8 over a range of temperatures and the results are shown in Table 1. The data shows that average pore width decreases from 38 nm at 10°C to 26 nm at 50°C. Thus, the variation of pore width with temperature follows the trend predicted by our model.

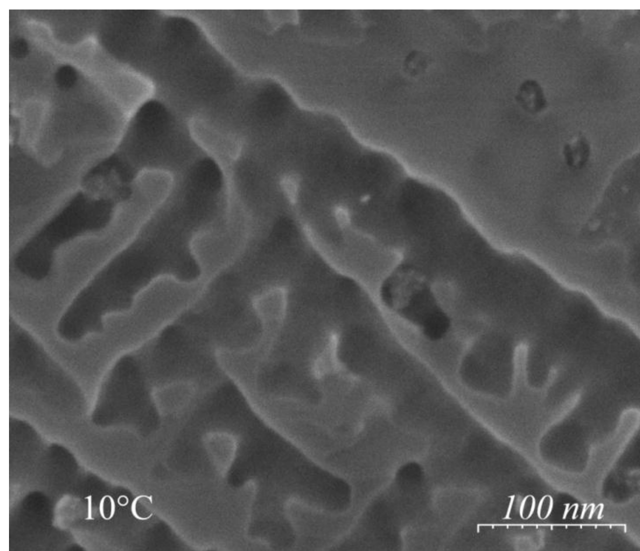


(a)

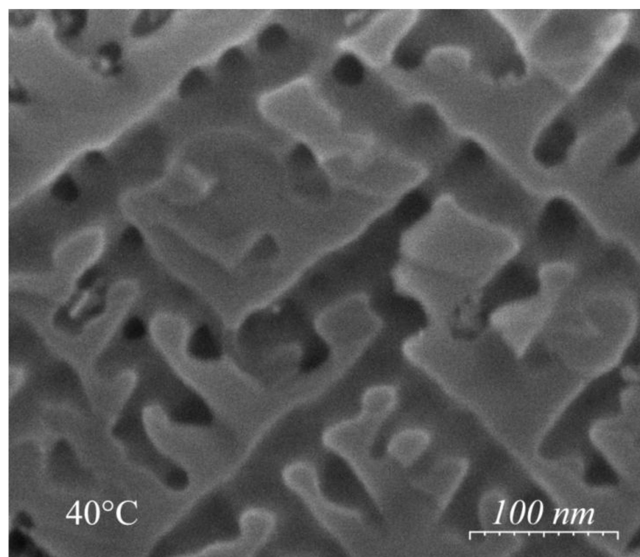


(b)

**Fig. 8** Cross-sectional (α) SEM images of pores formed in n-InP (n ≈ 5.3 × $10^{18}$ $cm^{-3}$) anodised by LPS from 0 V (SCE) to (a) 0.6 V and (b) 0.25 V at 2.5 mV $s^{-1}$ in 9 mol $dm^{-3}$ KOH. The experiments were performed at (a) 10°C and (b) 40°C as indicated. It can be seen that pores formed at the lower temperature are slightly wider.

The variation of pore width with carrier concentration was also investigated. Typical results for electrodes with three different carrier concentrations anodised in 5 mol $dm^{-3}$ KOH are shown in Table 2. The data shows that the average pore width decreases from 30 nm to 19 nm as the carrier concentration is increased from 3.4 × $10^{18}$ $cm^{-3}$ to 6.7 × $10^{18}$ $cm^{-3}$. The reduction in pore width with increasing carrier concentration can be explained by considering the effect on both $w_t$ and $\Delta w$. As already discussed, the tip width $w_t$ is determined primarily by the thickness of the depletion layer $x_{sc}$. Since the value of $x_{sc}$ at a given potential decreases with increasing carrier concentration, the radius of curvature of the pore tip must also decrease. This would lead to a decrease in pore width with increasing carrier concentration. The value of $\Delta w$ may also be affected by the thinner depletion layer. The model of Ostermeyer *et al.*[59] for hole diffusion and annihilation by electrochemical reaction during photoanodic etching showed that when holes are confined in a thinner near-surface region, their diffusion distance is shorter. Furthermore, as described by Blakemore,[62] impurity scattering associated with increased doping also significantly decreases the mobility of holes for dopant concentrations of greater than $10^{16}$ $cm^{-3}$. Thus, the thinner diffusion layer and greater scattering of carriers at higher carrier concentrations could decrease $\Delta w$.

**Table 2** Variation of pore width, surface pit diameter and near surface layer thickness with carrier concentration, for InP anodised by LPS at 2.5 mV $s^{-1}$ in 5 mol $dm^{-3}$ KOH at room temperature.

| Carrier Concentration / × $10^{18}$ $cm^{-3}$ | Pore Width / nm | Surface Pit Diameter / nm | Near-Surface Layer Thickness / nm |
|---|---|---|---|
| 3.4 | 30 | 14 | 45 |
| 5.3 | 28 | 17 | 39 |
| 6.7 | 19 | 22 | 34 |

We have also investigated the effect of electrolyte concentration on pore width. The observed variations are not as simple as in the case of temperature and will be described in detail elsewhere.[9] However, these results are also consistent with the effect of competition between reaction rate and diffusion as predicted by the model.

Thus, model predictions of the effect of temperature on pore width are supported by the experimental evidence. The observed variations of pore width with carrier concentration and electrolyte concentration are also consistent with the model.

### Pore Wall Thickness and Deviations of Pores from <111>A Directions

If holes did not diffuse a significant distance, the minimum distance between pores would be of the order of twice the thickness $x_{sc}$ of the depletion layer, since the tunnelling distance for hole generation would become prohibitively large if the depletion layers from adjacent pores overlapped. However, because hole diffusion broadens pores (by $\Delta w$ in Fig. 7) they can approach more closely. This additional distance is about $\Delta w/2$ in the case of a growing pore approaching an existing pore and about $\Delta w$ in the case of two growing pores approaching each other. The depletion layer thickness $x_{sc}$ is estimated to be ~20 nm for a typical InP electrode with a carrier concentration of 5 × $10^{18}$ $cm^{-3}$ at an applied potential of 0.4 V, based on a flat-band potential of -1.2 V (SCE) at pH 14,[63,64] and so pore wall thickness would be expected to be less than ~40 nm (*i.e.* $2x_{sc}$). Examination of micrographs such as those in Fig. 8 and Fig. 9 confirms that the pore wall thickness is indeed typically less than ~40 nm as predicted.

Measurements of pore wall thickness were obtained from micrographs of electrodes anodised in KOH for a range of electrolyte concentration and the results are plotted in Fig. 10.

Physical Chemistry Chemical Physics Accepted Manuscript


This journal is © The Royal Society of Chemistry [year]

View Article Online
DOI: 10.1039/C3CP52253A

The pore wall thickness is observed to increase with concentration of KOH from 14 nm at 2 mol dm$^{-3}$ to 40 nm at 10 mol dm$^{-3}$. It is likely that the kinetics of the electrochemical reaction increase with electrolyte concentration, decreasing the effective diffusion distance of holes. This would reduce the diffusion broadening of pores ($\Delta w$) and lead to thicker pore walls. It is noted in Fig. 10 that the pore wall thickness appears to plateau approaching a value of ~40 nm (~$2x_{sc}$).

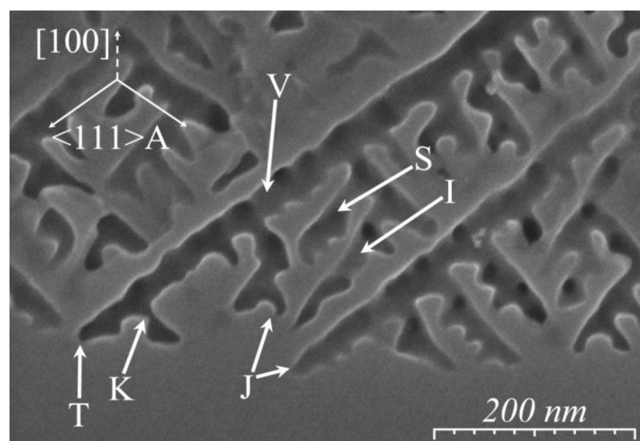


**Fig. 9** Cross-sectional (α) SEM image of n-InP (n ≈ 5.3 × 10$^{18}$ cm$^{-3}$) after an LPS from 0 to 0.383 V (SCE) in 5 mol dm$^{-3}$ KOH at 2.5 mV s$^{-1}$ at room temperature. A primary pore with a tip at T is indicated at V. Pores whose growth has been restricted are indicated at K and I (*i.e.* restricted by pores not seen in the image and by the pores indicated by J, respectively) while a pore that has diverged from V is indicated at S.

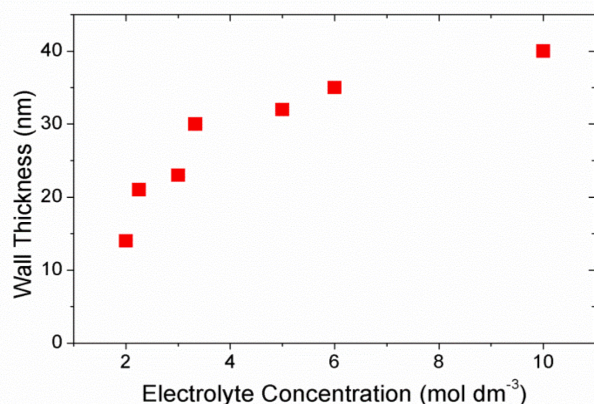


**Fig. 10** Plot of pore wall thickness against electrolyte concentration for porous n-InP layers (n ≈ 3.4 × 10$^{18}$ cm$^{-3}$) formed by LPS at 2.5 mV s$^{-1}$ in a range of KOH concentrations at room temperature.

If $\Delta w > 2x_{sc}$ (*e.g.* if the kinetics of the reaction are particularly slow), it is possible that pores may merge. The conditions for this can occur more easily in the case of a pore approaching another at an angle (rather than a case of two parallel pores) since the depletion layer is thinner at the pore tips than at the pore walls. Both the merging of parallel pores [10,41] and the crossing of pores which approach each other at an angle [3] have been reported.

In Figs. 2, 8 and 9, pores can be seen to sometimes deviate slightly from the <111>A directions. The pore propagation model can explain these deviations. As discussed earlier, symmetrical etching of the three {111}A facets forming the tip causes it to propagate in the fourth <111>A direction. If the carrier supply is diminished at any of the three tip facets, the etch rate at that facet decreases, causing the propagation of the pore tip to deviate in the direction away from that facet. The rate of hole generation at a pore tip will be reduced when it is in close proximity to the depletion region surrounding adjacent pores. The rate of hole generation will then become asymmetrical and consequently so will the supply of holes to the facets in Region 2 (Fig. 7), assuming that Region 1 is of significant width. This asymmetry in hole supply will redirect the pore away from adjacent pores and from its original <111>A growth direction.

Such a situation can be seen at F in Fig. 2b, where pores have veered away from the <111>A direction due to the depletion region at the electrode surface, so creating a non-porous near-surface layer ~40 nm thick. Table 2 shows values for the thickness of the near-surface layer for three different carrier concentrations. The thickness decreases with increasing carrier concentration, reflecting the corresponding decrease in depletion layer thickness. In Fig. 9, a pore S has diverged from the primary pore at V and a pore I that is restricted by neighbouring pores J has propagated into a bottle-neck resulting in a tapered shape. Also a pore at K branching from the pore V has narrowed, possibly due to the proximity of other pores in a parallel (011) plane and not visible in the image. Despite this narrowing, the pore attained a normal width after growing past the impeded region. Alternatively, the branching at K could have taken place in Region 3 or 4 (see Fig. 7), where the depletion layer is widening, resulting in an initially narrower pore due to a mechanism similar to the mechanism (described later) that dictates the formation of the channel from each surface pit.

## Pore Uniformity and Morphology

The model assumes that all etching is confined to a region in the vicinity of the tip of the pore. Therefore if etching conditions at the tip remain constant, no variation in pore width should be observed along its length. The microscopic evidence supports this prediction as discussed earlier.

The model also assumes <111>A facets near the pore tip. Although it is difficult to obtain clear-cut evidence, some TEM images tentatively support such faceting. Figure 11 shows two TEM images acquired after tilting the sample so as to observe the pore cross-sections as viewed along a zone axis equivalent to the <111>B direction. The pore cross-section in Fig. 11a passes close to the vertex of a porous domain and intersects a pore very close to its tip (at G). The light-grey area at G appears to form a triangle, the sides of which are approximately parallel to the intersections of the {111} planes with the image plane as shown in the inset. This suggests that the internal surface of the region in the vicinity of the tip of the pore consists of {111}A facets.

The cross-section shown in Fig. 11b intersects pores far from their tips. These cross-sections are quasi-circular and no faceting is apparent. In general, as far as can be determined, at extended distances from the pore tip, the pore cross-sections are round with no apparent facets. This round shape can be explained as resulting from the decrease in hole density with distance from the pore tip, causing the wall of the pore to curve towards the pore axis, away from the planes of the three {111}A faces (as shown in Fig. 7).

However for certain ranges of tip width $w_t$ and hole diffusion distance, it might be expected that the <111>A facets near the pore tips would lead to triangular pore cross-sections. We have

Published on 31 July 2013. Downloaded by University College Cork on 07/08/2013 15:00:57.

Physical Chemistry Chemical Physics Accepted Manuscript

View Article Online
DOI: 10.1039/C3CP52253A

Published on 31 July 2013. Downloaded by University College Cork on 07/08/2013 15:00:57.

observed pores with triangular cross-section when InP is anodised in KOH at very low current densities (<10 mA cm$^{-2}$). Faceted pore cross sections are commonly observed, both for III-V semiconductors in HCl [46,65] and for silicon in HF.[47] Thus, the model can explain both the round cross sections usually observed in InP in KOH and faceted pores which are also observed.

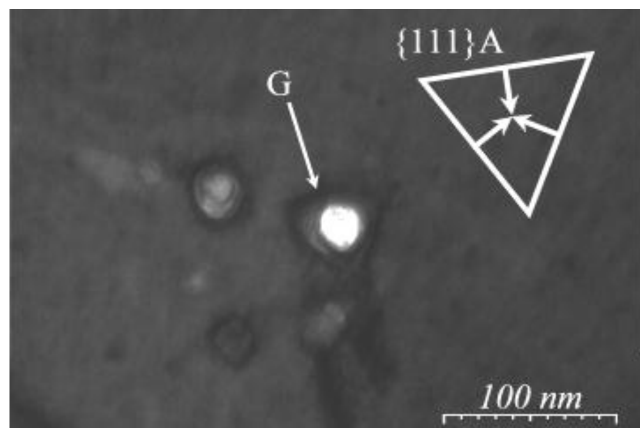


(a)

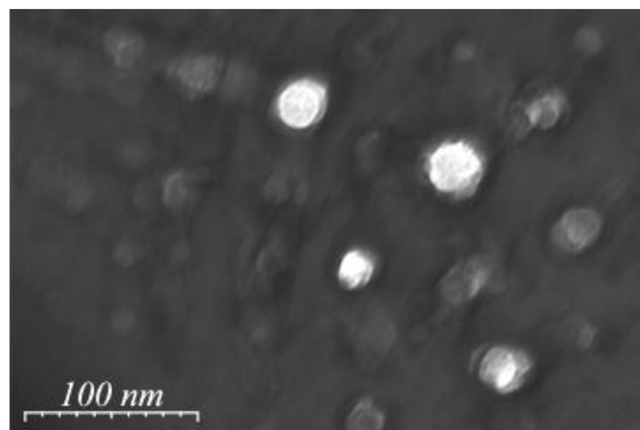


(b)

**Fig. 11** TEM images, viewed along a <111>B direction, of a β-plane slice of n-InP (n ≈ 3.4 × 10$^{18}$ cm$^{-3}$). The cross-section in (a) passes through a pore close to its tip (at G) while the cross-section in (b) passes through pores far from their tips. The electrode was anodised by an LPS from 0 to 0.44 V (SCE) in 5 mol dm$^{-3}$ KOH at 2.5 mV s$^{-1}$ at room temperature. The FIB-milled InP slice is ~100 nm thick.

### Initiation and Termination of Pore Growth

Pores begin at a pit on the electrode surface. Such pits are expected to form by electrochemical etching at surface 'defects' such as, for example, localized nano-scale regions of impurity or high carrier concentration.[55,56] Once a pit is formed, the small radius of curvature and consequent high electric field at its tip will enable hole generation causing it to etch further. Hole generation can occur only by tunnelling paths at small angles to the surface normal, because of the geometry of the depletion layer boundary as shown in Fig. 12a. Thus, etching at the surface pit is constrained to be normal to the surface causing the formation of a very narrow channel, as shown in the schematic of Fig. 12b and observed in the SEM image of Fig. 12e. When a pit has grown a certain distance, the depletion region bulges inward sufficiently that carriers become available towards the sides of the pit. This allows {111}A-oriented facets to be revealed, forming a shape similar to a truncated tetrahedron, the two vertices of which become the tips of primary pores (Fig. 12c). These then propagate along <111>A directions as shown in Fig. 12d.

The diameter of a surface pit increases with increasing carrier concentration, as shown in Table 2. This variation appears to reflect the corresponding decrease in depletion layer thickness which results in pits branching and widening at a shallower depth.

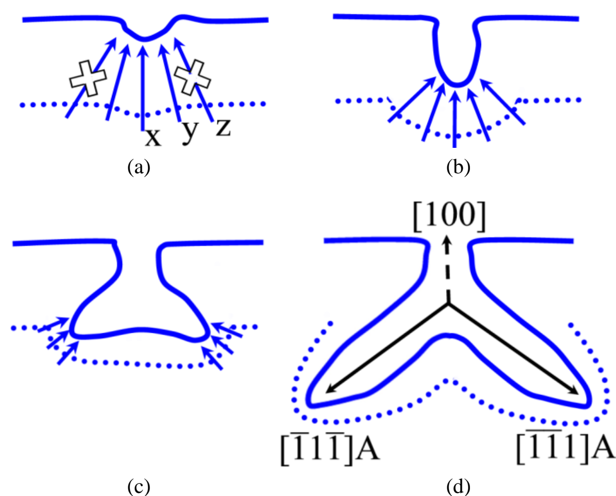


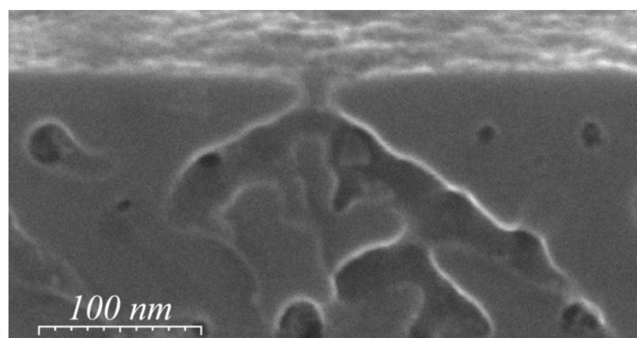


(e)

**Fig. 12** Schematic representation of the progression of etching from a pit in the surface. (a) The pit initially etches vertically due to availability of holes by paths x and y but not z. (b) The channel lengthens in the [1̄00] direction. (c) Once the channel is deep enough, the availability of carriers to the sides allows some lateral etching. This etching widens the end of the channel into a truncated tetrahedral void that produces (d) two primary pores when the void is sufficiently large. (e) The model can be directly compared to experimental observation of two <111>A pores extending from a pit in the electrode surface in an α-plane SEM cross-section of n-InP (n ≈ 3.4 × 10$^{18}$ cm$^{-3}$) after an LPS from 0 to 0.6 V (SCE) in 5 mol dm$^{-3}$ KOH at 2.5 mV s$^{-1}$ at room temperature.

For many semiconductor/electrolyte combinations, porous layers can be readily etched many tens of microns into the substrate, notably for InP etched in HCl.[46,66] For porous InP formed in KOH however, porous layer growth typically terminates at a relatively small thickness (~3 μm).[67] This limited thickness (*i.e.* early termination of porous layer growth) is likely due to the specific chemistry of the etching reaction in the KOH electrolyte.

Reports of electrochemical etching of InP in a range of electrolytes have variously suggested a process involving 6 or 8

Physical Chemistry Chemical Physics Accepted Manuscript

 This journal is © The Royal Society of Chemistry [year]

Published on 31 July 2013. Downloaded by University College Cork on 07/08/2013 15:00:57.

electrons [68-74] (or holes) which may be represented as

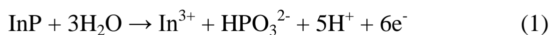

$$InP + 3H_2O \rightarrow In^{3+} + HPO_3^{2-} + 5H^+ + 6e^- \quad (1)$$

or

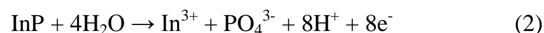

$$InP + 4H_2O \rightarrow In^{3+} + PO_4^{3-} + 8H^+ + 8e^- \quad (2)$$

We have determined the number of electrons involved in the electrochemical etching of InP in KOH from the charge passed and the corresponding layer thickness and porosity (*i.e.* volume fraction of pores) estimated from SEM cross sections. To estimate the porosity we measured the areal density and dimensions of through-plane pores in SEM cross-sections of both α and β cleavage planes and assumed an ideal pore geometry (uniformly spaced cylindrical pores along <111>A directions). In a typical experiment, InP was anodized at 20 mA $cm^{-2}$ in 5 mol $dm^{-3}$ KOH for 70 s and a 3.0-μm layer was obtained with a porosity estimated to be 0.24. These values correspond to an average of ~6 electrons per formula unit of InP, assuming a mol volume [75] of 30.31 $cm^3$ $mol^{-1}$. Further details of these measurements will be published elsewhere.

$In^{3+}$ ions are unstable at higher pH with respect to precipitation as hydroxides, oxides or oxyhydroxides. However, like other group III elements, indium has amphoteric character and has some solubility in strong alkali as $InO_2^-$.[76] Thus the etching of InP in high concentrations of KOH may proceed by a process such as

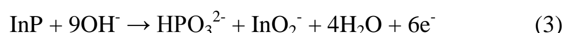

$$InP + 9OH^- \rightarrow HPO_3^{2-} + InO_2^- + 4H_2O + 6e^- \quad (3)$$

There are reports [76] that the dissolved indium species can reprecipitate from alkali solution after a certain time.

The porous layer is connected to the bulk electrolyte through a small number of surface pits (one for each porous domain formed initially) through which the reaction products from all of the etching pore tips must be transported. There is some evidence that this mass transport bottleneck eventually leads to precipitation of reaction products within the pores. A precipitated solid, which appears from energy dispersive x-ray spectroscopy (EDX) and electron diffraction measurements to be largely $In_2O_3$, is commonly observed within the porous structure and on the surface of porous layers which have been grown to the point of termination. These precipitates can block the narrow diffusion pathways between the pore tips and the bulk electrolyte. It seems likely that such a process is responsible for the termination of pore etching in InP in KOH.

## Conclusions

We propose a three-step model of electrochemical nanopore formation that explains how crystallographically oriented etching can occur even though the rate-determining process (hole generation) occurs only at pore tips.

Step 1 is the generation of holes at pore tips under the influence of a high electric field due to the small radius of curvature at the pore tip. Step 2 is the diffusion of holes parallel to the surface of the semiconductor, enabling the electrochemical etching reaction to occur some distance from the pore tip where the holes are created. Step 3 is the actual electrochemical reaction itself.

Step 1 determines the overall etch rate. However, competition in kinetics between hole diffusion (Step 2) and electrochemical reaction (Step 3) determines the average diffusion distance of holes and this in turn determines whether etching is crystallographic. If the kinetics of Step 3 are slow relative to Step 2, then etching can occur at preferred crystallographic sites, such as phosphorus dangling bonds in InP, within a zone in the vicinity of the pore tip and this will lead to pore propagation in preferential directions.

Under these conditions, etching will eventually reveal the slow etching {111}A facets to form a pyramidal pore tip. Indium vacancy sites formed on these facets expand by rapid two-dimensional etching along the surface to expose the next {111}A plane. Thus, in the vicinity of the pore tip, the {111}A faces are etched, one monolayer at a time, so that the tip region maintains its pyramidal shape, and so the tip remains sharp as it propagates. Symmetrical etching of the three {111}A faces forming the tip causes it to propagate in the (fourth) <111>A direction. As a pore etches, propagating atomic ledges can meet to form sites that can become new pore tips and this enables branching of pores along any of the <111>A directions.

Model predictions of the effect of temperature on pore width are supported by the experimental evidence. The observed uniform width of pores and its variation with carrier concentration and electrolyte concentration is also consistent with the model. The model can also account for pore wall thickness and observed deviations of pore propagation from the <111>A directions.

TEM observations tentatively confirm the presence of faceted pore tips, as postulated by the model. The observed morphology and dimensions of the surface pits from which nanopores begin are also explained and factors leading to pore growth termination are discussed in terms of the chemistry of the etch products.

Finally, it is observed that the InP/KOH system is an ideal candidate for the study of purely electrochemical nanopore formation in that all of the etching appears to be confined to the pore tip region with no chemical etching taking place at the pore walls after the tip has moved on. However, we believe that the model is generally applicable to electrochemical pore formation in III-V semiconductors and should lead towards greater control of porous structures.

## Acknowledgment

R. P. Lynch and N. Quill would like to thank the Irish Research Council (IRC) for PhD scholarships to perform this research. R. P. Lynch acknowledges a joint IRC - Marie Curie Fellowship under grant no. INSPIRE PCOFUND-GA-2008-229520. The authors would also like to acknowledge the support of the Tyndall National Institute. This support was provided through the Science Foundation Ireland (SFI) funded National Access Programme (Project NAP No. 37 and 70)

## Notes and References

[a] *Department of Physics and Energy, Materials and Surface Science Institute, University of Limerick, Ireland. Fax: +353-61-202423; Tel: +353-61-234705; E-mail: Robert.Lynch@UL.ie*
[b] *Department of Chemistry and Tyndall National Institute, University College Cork, Ireland.*

1 T. Kalil *et al.*, *Supplement to the President's Budget for Fiscal Year 2014 – The National Nanotechnology Initiative*, Subcommittee on Nanoscale Science, Engineering, and Technology Committee on

Physical Chemistry Chemical Physics Accepted Manuscript

View Article Online
DOI: 10.1039/C3CP52253A

Published on 31 July 2013. Downloaded by University College Cork on 07/08/2013 15:00:57.

Technology National Science and Technology, United States of America, 2013, pg. 7 - 40
2 R. L. Smith and S. D. Collins, *J. Appl. Phys.*, 1992, **71**, 8
3 S. Langa, J. Carstensen, M. Christophersen, H. Föll and I. M. Tiginyanu, *Appl. Phys. Lett.*, 2001, **78**, 1074
4 G. Oskam, A. Natarajan, P. C. Searson and F. M. Ross, *Appl. Surf. Sci*., 1997, **119,** 160
5 S. Langa, J. Carstensen, I. M. Tiginyanu, M. Christophersen and H. Föll, *Electrochem. Solid-State Lett.*, 2001, **4**, G50
6 S. Langa, I. M. Tiginyanu, J. Carstensen, M. Christophersen and H. Föll, *Electrochem. Solid-State Lett.*, 2000, **3**, 514
7 P. Schmuki, J. Fraser, C. M. Vitus, M. J. Graham and H. S. Isaacs, *J. Electrochem. Soc.*, 1996, **143,** 3316
8 P. Schmuki, D. J. Lockwood, J. Fraser, M. J. Graham and H. S. Isaacs, *Mater. Res. Soc. Symp. Proc.*, 1996, **431,** 439
9 N. Quill, R. P. Lynch, C. O'Dwyer and D. N. Buckley, *ECS Trans.,* 2013, **50 (37)**, 131
10 N. Quill, R. P. Lynch, C. O'Dwyer and D. N. Buckley, *ECS Trans.*, 2013, **50 (6)**, 377
11 A.-M. Gonçalves, L. Santinacci, A. Eb, I. Gerard, C. Mathieu and A. Etcheberry, *Electrochem. Solid-State Lett.*, 2007, **10**, D35
12 R. P. Lynch, C. O'Dwyer, D. N. Buckley, D. Sutton and S. B. Newcomb, *ECS Trans.*, 2006, **2,** 131
13 M. Christopherson, J. Carstensen, A. Feuerhake and H. Föll, *Mater. Sci. Eng. B*, 2000, **69-70**, 194
14 S. Rönnebeck, J. Carstensen, S. Ottow and H. Föll, *Electrochem. Solid-State Lett.*, 1999, **2**, 126
15 P. Schmuki, L. E. Erickson, D. J. Lockwood, J. W. Fraser, G. Champion and H. J. Labbé, *Appl. Phys. Lett*., 1998, **72**, 1039
16 V. Lehmann and H. Föll, *J. Electrochem. Soc.*, 1990, **137**, 653
17 T. Unagami, *J. Electrochem. Soc.*, 1980, **127**, 476
18 J. Carstensen, M. Christophersen and H. Föll, *Mater. Sci. Eng. B*, 2000, **69-70**, 23
19 F. M. Ross, G. Oskam, P. C. Searson, J. M. Macaulay and J. A. Liddle, *Philos. Mag. A*, 1997, **75**, 525
20 M. J. J. Theunissen, *J. Electrochem. Soc.*, 1972, **119**, 351
21 M. I. J. Beale, J. D. Benjamin, M. J. Uren, N. G. Chew and A. G. Cullis, *J. Cryst. Growth*, 1985, **73**, 622
22 P. Allongue, C. H. de Villeneuve, L. Pinsard and M. C. Bernard, *Appl. Phys. Lett.*, 1995, **67**, 941
23 V. Lehmann and U. Gösele, *Appl. Phys. Lett.*, 1991, **58**, 8
24 J.-N. Chazalviel, R. B. Wehrspohn and F. Ozanam, *Mater. Sci. Eng. B*, 2000, **69-70**, 1
25 J.-N. Chazalviel, F. Ozanam, N. Gabouze, S. Fellah and R. B. Wehrspohn, *J. Electrochem. Soc.*, 2002, **149**, C511
26 X. G. Zhang, *J. Electrochem. Soc.*, 1991, **138**, 3750
27 X. G. Zhang, *J. Electrochem. Soc.*, 2004, **151**, C69
28 M. Kappelt and D. Bimberg, *J. Electrochem. Soc.*, 1996, **143**, 3271
29 H. C. Gatos and M. J. Lavine, *J. Electrochem. Soc.*, 1960, **107**, 427
30 H. H. Goossens and W. P. Gomes, *J. Electrochem. Soc.*, 1991, **138**, 1696
31 S. N. G. Chu, C.M. Jodlauk and W.D. Johnston Jr., *J. Electrochem. Soc.*, 1983, **130**, 2399
32 D. Soltz and L. Cescato, *J. Electrochem. Soc.*, 1996, **143**, 2815
33 M. M. Carrabba, N. M. Nguyen and R. D. Rauh, *J. Electrochem. Soc.*, 1987, **134**, 1855
34 P. H. L. Notten, *J. Electrochem. Soc.*, 1991, **138**, 243
35 I. E. Vermeir, W. P. Gomes and P. van Daele, *J. Electrochem. Soc.*, 1995, **142**, 3226
36 Y. Tarui, Y. Komiya and Y. Harada, *J. Electrochem. Soc.*, 1971, **118**, 118
37 S. Adachi and K. Oe, *J. Electrochem. Soc.*, 1983, **130**, 2427
38 R. P. Lynch, C. O'Dwyer, N. Quill, S. Nakahara, S.B. Newcomb and D. N. Buckley, *J. Electrochem. Soc.*, 2013, **160**, D260
39 R. P. Lynch, C. O'Dwyer, D. Sutton, S. B. Newcomb and D. N. Buckley, *ECS Trans.*, 2007, **6 (2)**, 355
40 C. O'Dwyer, D. N. Buckley, D. Sutton, M. Serantoni and S. B. Newcomb, *J. Electrochem. Soc.*, 2007, **154**, H78
41 N. Quill, R. P. Lynch, C. O'Dwyer and D. N. Buckley, *ECS Trans.*, 2013, **50 (37)**, 143
42 C. O'Dwyer, D. N. Buckley, D. Sutton and S. B. Newcomb, *J. Electrochem. Soc.*, 2006, **153**, G1039
43 R. P. Lynch, M. Dornhege, P. Sánchez-Bodega, H. H. Rotermund and D. N. Buckley, *ECS Trans.*, 2007, **6 (2)**, 331
44 R. P. Lynch, C. O'Dwyer, D. N. Buckley, D. Sutton and S. B. Newcomb, *ECS Trans.*, 2006, **2,** 131
45 L. A. Giannuzzi and F. A. Stevie, *Micron.*, 1999, **30**, 197
46 E. Spiecker, M. Rudel, W. Jäger, M. Leisner and H. Föll, *Phys. Stat. Sol. (a)*, 2005, **202,** 2950
47 T. Osaka, K. Osgasawara and S. Nakahara, *J. Electrochem. Soc.*, 1991, **144**, 3750
48 J. McHardy and F. Ludwig, *Electrochemistry of Semiconductors and Electronics: Processes and Devices*, Noyes Publications, 1992, pg. 182
49 S.-M. Park and M. E. Barber, *J. Electroanal. Chem.*, 1979, **99**, 67
50 H. Gerischer, *J. Electroanal. Chem.*, 1977, **82**, 133
51 W. P. Gomes and H. H. Goossens, *Advances in Electrochemical Science and Engineering*, Wiley-VCH, 1994, 3, pg. 8
52 S. R. Morrison, *Electrochemistry at semiconductor and oxidized metal electrodes*, Plenum Press, 1980, pg. 238
53 H. Föll, M. Christophersen, J. Carstensen and G. Hasse, *Phys. Stat. Sol. (a)*, 2000, **182**, 7
54 V. P. Parkhutik, L. K. Glinenko and V. A. Labunov, *Surf. Tech.*, 1983, **20**, 265
55 P. Schmuki, L. E. Erickson, D. J. Lockwood, B. F. Mason, J. W. Fraser, G. Champion, and H. J. Labbe, *J. Electrochem. Soc.*, 1999, **146**, 735
56 I. M. Tiginyanu, C. Schwab, J.-J. Grob, B. Prévot, H. L. Hartnagel, A. Vogt, G. Irmer and J. Monecke, *Appl. Phys. Lett.*, 1997, **71**, 3829
57 R. W. Tjerkstra, J. Gómez Rivas, D. Vanmaekelbergh and J. J. Kelly, *Electrochem. Solid-State Lett.*, 2002, **5**, G32
58 H. C. Gatos and M. C. Lavine, *J. Phys. Chem. Solids*, 1960, **14**, 169
59 F. W. Ostermayer, P. A. Kohl, R. M. Lum, *J. Appl. Phys.*, 1985, **58**, 4390
60 S. W. Benson, *The Foundations of Chemical Kinetics*, McGraw-Hill, 1960, pg. 31
61 D. N. MacFayden, *J. Electrochem. Soc.*, 1983, **130**, 1934
62 J. S. Blakemore, *J. Appl. Phys.*, 1982, **53**, R123
63 S. Qian, D. Qian and B. Sun, *Acta Chimica Sinica*, 1983, **1**, 2
64 J. Schefold, *J. Electrochem. Soc.*, 1992, **139**, 2862
65 S. Langa, J. Carstensen, I. M. Tiginyanu, M. Christophersen and H. Föll, *Electrochem. Solid-State Lett.*, 2002, **5**, C14
66 L. Santinacci, A. M. Gonçalves and A. Etcheberry, *ECS Trans.*, 2007, **6 (2)**, 323
67 R. P. Lynch, N. Quill, C. O'Dwyer, M. Dornhege, H. H. Rotermund and D. N. Buckley, *ECS Trans.*, 2013, **53 (6)**, 65
68 H. Gerischer and W. Mindt, *Electrochim. Acta*, 1968, **13**, 1329
69 A. B. Ellis, J. M. Bolts and M. S. Wrighton, *J. Electrochem. Soc.*, 1977, **124**, 1603
70 M. M. Faktor, T. Ambridge, C. R. Elliott and J. C. Regnault, *Curr. Top. Mater. Sci.*, 1980, **6**, 1
71 P. A. Kohl, C. Wolowodiuk and F. W. Ostermayer, *J. Electrochem. Soc.*, 1983, **130**, 2288
72 S. Preusser, M. Herlem, A. Etcheberry and J. Jaume, *Electrochim. Acta*, 1992, **37**, 289
73 L. Santinacci, M. Bouttemy, I. Gerard and A. Etcheberry, *ECS Trans.*, 2009, **19**, 313
74 Z. Weng, A. Liu, Y. Sang, J. Zhang, Z. Hu, Y. Liu and W. Liu, *J. Porous Mater.*, 2009, **16**, 707
75 D. L. Lide, *CRC Handbook of Chemistry and Physics 86th ed.: Physical Constants of Inorganic Compounds*, CRC Press, New York 2005, pg. 4-65
76 M. Pourbaix, *Atlas of Electrochemical Equilibria in Aqueous Solutions*, 2nd English Ed., National Association of Corrosion Engineers, 1974, pg. 439

Physical Chemistry Chemical Physics Accepted Manuscript

 This journal is © The Royal Society of Chemistry [year]